Preparation of Mesoporous Silica Films with Fully Aligned Large Mesochannels Using Nonionic Surfactants

Hirokatsu Miyata,*,† Takashi Noma,† Masatoshi Watanabe,† and Kazuyuki Kuroda‡,§

Canon Inc. Core-Technology Development Headquarters Canon Research Center, 5-1, Morinosato-Wakamiya, Atsugi-shi, Kanagawa 243-0193, Japan, Department of Applied Chemistry, Waseda University, Ohkubo-3, Shinjuku-ku, Tokyo 169-8555, Japan, and Kagami Memorial Laboratory for Materials Science and Technology, Waseda University, Nishiwaseda-2, Shinjuku-ku, Tokyo 169-0051, Japan

Received September 7, 2001

Mesoporous silica films with uniaxially aligned large-sized mesochannels were prepared using nonionic alkyl poly(ethylene oxide) surfactants and a rubbing-treated polyimide coating. Although the increment of the pore size was small as long as conventional alkylammonium surfactants were used, the use of nonionic surfactants with poly(ethylene oxide) headgroups led to successful enlargement of the mesochannels. The directional distribution of the mesochannels in the films, which is estimated by in-plane X-ray diffraction, was very narrow and was comparable with that in the oriented mesostructured silica films prepared using hexadecyltrimethylammonium chloride as a templating agent. The distribution of the alignment direction of the mesochannels is nearly independent of the nature of the hydrophilic headgroup, but is slightly affected by the alkyl-chain length of the surfactants used. These results indicate that the alignment of the mesochannels is determined by the hydrophobic interactions between the oriented polymer chains of the rubbed polyimide and the surfactant tail groups.

Introduction

Because of the large demands for new molecular devices, nanoscaled structural control of materials is one of the most important issues in the technologies of the 21st century. Among the various methods for achieving this aim, the strategies based on host−guest chemistry are promising because of the ease and the cost of the processes.[1−3] In this strategy, various guest species such as molecules,[4−11] clusters,[12−18] and metals[19−22] are incorporated into the nanospaces of host materials, and the ordering of the guests can be realized using well-ordered host materials. The consequent size effect and isolation effect of incorporated guest species often lead to the appearance of peculiar properties that are never observed in bulk materials.[5−8,12]

Mesoporous materials synthesized through self-assembling of surfactants are of special interest as host materials because of their highly ordered porous

* To whom correspondence should be addressed. E-mail: miyata.hirokatsu@canon.co.jp.

† Canon Inc. Core-Technology Development Headquarters Canon Research Center.

‡ Department of Applied Chemistry, Waseda University.

§ Kagami Memorial Laboratory for Materials Science and Technology, Waseda University.

(1) Alberti, G.; Bein, T. *Comprehensive Supramolecular Chemistry, volume 7, Solid-State Supramolecular Chemistry: Two- and Three-Dimensional Inorganic Networks*; Elsevier Science: London, 1996.

(2) Schöllhorn, R. *Chem. Mater.* **1996**, *8*, 1747.

(3) Moller, K.; Bein, T. *Chem. Mater.* **1998**, *10*, 2950.

(4) (a) Wu, C.-G.; Bein, T. *Chem. Mater.* **1994**, *6*, 1109. (b) Wu, C.-G.; Bein, T. *Science* **1994**, *264*, 1757.

(5) Nguyen, T.-Q.; Wu, J.; Doan, V.; Schwartz, B. J.; Tolbert, S. H. *Science* **2000**, *288*, 652. (b) Wu, J.; Gross, A. F.; Tolbert, S. H. *J. Phys. Chem. B* **1999**, *103*, 2374.

(6) Marlow, F.; McGehee, M. D.; Zhao, D.; Chmelka, B. F.; Stucky, G. D. *Adv. Mater.* **1999**, *11*, 632.

(7) Yang, P.; Wirnsberger, G.; Huang, H. C.; Cordero, S. R.; McGehee, M. D.; Scott, B.; Deng, T.; Whitesides, G. M.; Chmelka, B. F.; Buratto, S. K.; Stucky, G. D. *Science* **2000**, *287*, 465.

(8) Wirnsberger, G.; Stucky, G. D. *Chem. Mater.* **2000**, *12*, 2525.

(9) Ogawa, M.; Nakamura, T.; Mori, J.; Kuroda, K. *J. Phys. Chem. B* **2000**, *104*, 8554.

(10) Furukawa, H.; Kuroda, K.; Watanabe, T. *Chem. Lett.* **2000**, 1256.

(11) Wirnsberger, G.; Scott, B. J.; Chmelka, B. F.; Stucky, G. D. *Adv. Mater.* **2000**, *12*, 1450.

(12) (a) Dag, Ö.; Kuperman, A.; Ozin, G. A. *Adv. Mater.* **1995**, *7*, 72. (b) Chomski, E.; Dag, Ö.; Kuperman, A.; Coombs, N.; Ozin, G. A. *Chem. Vap. Deposition* **1996**, *2*, 8. (c) Dag, Ö.; Ozin, G. A.; Yang, H.; Reber, C.; Bussière, G. *Adv. Mater.* **1999**, *11*, 474.

(13) Leon, R.; Margolese, D.; Stucky, G.; Petroff, P. M. *Phys. Rev. B: Condens. Matter* **1995**, *52*, r2285.

(14) Srdanov, V. I.; Alxneit, I.; Stucky, G. D.; Reaves, C. M.; DenBaars, S. P. *J. Phys. Chem. B* **1998**, *102*, 3341.

(15) Tang, Y. S.; Cai, S.; Jin, G.; Duan, J.; Wang, K. L.; Soyez, H. M.; Dunn, B. S. *Appl. Phys. Lett.* **1997**, *71*, 2448.

(16) Agger, J. R.; Anderson, M. W.; Pemble, M. E.; Terasaki, O.; Nozue, Y. *J. Phys. Chem. B* **1998**, *102*, 3345.

(17) Winkler, H.; Brinker, A.; Hagan, V.; Wolf, I.; Schmechel, R.; von Seggern, H.; Fischer, R. A. *Adv. Mater.* **1999**, *11*, 1444.

(18) Coleman, N. R. B.; Morris, M. A.; Spalding, T. R.; Holmes, J. D. *J. Am. Chem. Soc.* **2001**, *123*, 187.

(19) (a) Liu, Z.; Sakamoto, Y.; Ohsuna, T.; Hiraga, K.; Terasaki, O.; Ko, C. H.; Shin, H. J.; Ryoo, R. *Angew. Chem., Int. Ed.* **2000**, *39*, 3107. (b) Shin, H. J.; Ryoo, R.; Liu, Z.; Terasaki, O. *J. Am. Chem. Soc.* **2001**, *123*, 1246. (c) Liu, Z.; Terasaki, O.; Ohsuna, T.; Hiraga, K.; Shin, H. J.; Ryoo, R. *Chem. Phys. Chem.* **2001**, *2*, 231.

(20) (a) Lee, K.-B.; Lee, S.-M.; Cheon, J. *Adv. Mater.* **1999**, *13*, 517. (b) Kang, H.; Jun, Y−w.; Park, J.-I.; Lee, K.-B.; Cheon, J. *Chem. Mater.* **2000**, *12*, 3530.

(21) Plyuto, Y.; Berquier, J.-M.; Jacquiod, C.; Ricolleau, C. *Chem. Commun.* **1999**, 1653.

(22) Fukuoka, A.; Sakamoto, Y.; Guan, S.; Inagaki, S.; Sugimoto, N.; Fukushima, Y.; Hirahara, K.; Iijima, S.; Ichikawa, M. *J. Am. Chem. Soc.* **2001**, *123*, 3373.

10.1021/cm010412m CCC: $22.00
Published on Web 01/22/2002

structures[23−28] and controllability of morphologies.[29] Among the various morphologies, such as spheres,[30−34] fibers,[35−39] rods,[40,41] and monoliths,[42−45] thin films[46−57] of mesoporous materials are most promising for optical and electronic applications by incorporating various guest species. Especially, mesoporous films in which the orientation of the mesopores is precisely controlled at a macroscopic scale[56,57] are ideal host materials.

To control the porous structure of mesoporous materials, various methods have been proposed. Tolbert et al. reported the alignment of mesochannels using a magnetic field,[42] and several groups reported the alignment using a reactant flow.[58−60] On the other hand, mesochannels in mesostructured silica films can be aligned on crystalline substrates with anisotropic surfaces.[49−51,56] Recently, we developed a new method for aligning the mesochannels in mesoporous silica films using polymer coatings with a structural anisotropy such as Langmuir−Blodgett film[61] and rubbing-treated polyimide films[39,57,62] and achieved high uniaxial alignment of mesochannels. In this method, the mesostructured silica films are formed through heterogeneous nucleation and growth of the mesostuctured silica seeds, and the mesochannels in films are aligned through interactions at solid−liquid interfaces.

Although a cationic surfactant, hexadecyltrimethylammonium chloride ($CH_3(CH_2)_{15}N(CH_3)_3Cl$, abbreviated as $C_{16}TAC$), has been commonly used in previous reports, mesoporous silica films with an aligned channel structure become more useful when the pore size can be controlled. The solvent evaporation method, by which precise control of mesochannel alignment cannot be achieved, allows the use of a wide variety of surfactants such as amphiphilic triblock copolymers to obtain mesoporous silica films with large mesopores.[54] However, the surfactants applicable to the present method are very limited because the present method requires additional optimum interactions between the substrate surface and the surfactant. Therefore, the selection of appropriate surfactants and the reaction conditions are essential for the formation of mesostructured silica films with uniaxially aligned large mesochannels.

In this paper, we report the successful preparation of mesoporous silica films with highly aligned large-sized mesochannels through a combination of nonionic surfactants, $C_{12}H_{25}(OCH_2CH_2)_{10}OH$ and $C_{16}H_{33}(OCH_2CH_2)_{10}OH$ (abbreviated as $C_{12}EO_{10}$ and $C_{16}EO_{10}$, respectively), and a rubbing-treated polyimide coating. The pore size in the film prepared using $C_{16}EO_{10}$ was 13 Å larger than that in the film prepared using $C_{16}TAC$, and such large mesopores are never obtained as long as alkylammonium surfactants are used. The detailed study of in-plane XRD shows that the alignment of the mesochannels is independent of the nature of the hydrophilic headgroups of the surfactants and is determined by hydrophobic interactions between the surfactant tail groups and the oriented polymer chains of the polyimide film.

Experimental Section

Preparation of the Substrate. A clean silica glass substrate was coated with a polyimide precursor, polyamic acid,

(23) Yanagisawa, T.; Shimizu, T.; Kuroda, K.; Kato, C. *Bull. Chem. Soc. Jpn.* **1990**, *63*, 988.
(24) Inagaki, S.; Fukushima, Y.; Kuroda, K. *J. Chem. Soc., Chem. Commun.* **1993**, 680.
(25) Kresge, C. T.; Leonowicz, M. E.; Roth, W. J.; Vartuli, J. C.; Beck, J. S. *Nature* **1992**, *359*, 710.
(26) Beck, J. S.; Vartuli, J. C.; Roth, W. J.; Leonowicz, M. E.; Kresge, C. T.; Schmitt, K. D.; Chu, C. T−W.; Olson, D. H.; Sheppard, E. W.; McCullen, S. B.; Higgins, J. B.; Schlenker, J. L. *J. Am. Chem. Soc.* **1992**, *114*, 10834.
(27) (a) Huo, Q.; Margolese, D. I.; Ciesla, U.; Feng, P.; Gier, T. E.; Sieger, P.; Leon, R.; Petroff, P. M.; Schuth, F.; Stucky, G. D. *Nature* **1994**, *368*, 317. (b) Huo, Q.; Margolese, D. I.; Ciesla, U.; Demuth, G. D.; Feng, P.; Gier, T. E.; Sieger, P.; Firouzi, A.; Chmelka, B. F.; Schuth, F.; Stucky, G. D. *Chem. Mater.* **1994**, *6*, 1176.
(28) (a) Zhao, D.; Feng, J.; Huo, Q.; Melosh, N.; Fredrickson, G. H.; Chmelka, B. F.; Stucky, G. D. *Science* **1998**, *279*, 548. (b) Zhao, D.; Huo, Q.; Feng, J.; Chmelka, B. F.; Stucky, G. D. *J. Am. Chem. Soc.* **1998**, *120*, 6024.
(29) Ozin, G. A. *Chem. Commun.* **2000**, 419.
(30) Yang, H.; Vovk, G.; Coombs, N.; Sokolov, I.; Ozin,G. A. *J. Mater. Chem.* **1998**, *8*, 743.
(31) Huo, Q.; Feng, J.; Schüth, F.; Stucky, G. D. *Chem. Mater.* **1997**, *9*, 14.
(32) Grün, M.; Lauer, I.; Unger, K. K. *Adv. Mater.* **1997**, *9*, 254.
(33) Boissière, C.; van der Lee, A.; El Mansouri, A.; Larbot, A.; Prouzet, E. *Chem. Commun.* **1999**, 2047.
(34) Lu, Y.; Fan, H.; Stump, A.; Ward, T. L.; Rieker, T.; Brinker, C. J. *Nature* **1999**, *398*, 223.
(35) Yang, P.; Zhao, D.; Chmelka, B. F.; Stucky, G. D. *Chem. Mater.* **1998**, *10*, 2033.
(36) Huo, Q.; Zhao, D.; Feng, J.; Weston, K.; Buratto, S. K.; Stucky, G. D.; Schacht, S.; Schüth, F. *Adv. Mater.* **1997**, *9*, 974.
(37) Bruinsma, P. J.; Kim, A. Y.; Liu, J.; Baskaran, S. *Chem. Mater.* **1997**, *9*, 2507.
(38) (a) Marlow, F.; Spliethoff, B.; Tesche, B.; Zhao, D. *Adv. Mater.* **2000**, *12*, 961. (b) Marlow, F.; Leike, I.; Weidenthaler, C.; Lehmann, C. W.; Wilczok, U. *Adv. Mater.* **2001**, *13*, 307.
(39) Miyata, H.; Kuroda, K. *Adv. Mater.* **2001**, *13*, 558.
(40) Schmidt-Winkel, P.; Yang, P.; Margolese, D. I.; Chmelka, B. F.; Stucky, G. D. *Adv. Mater.* **1999**, *11*, 303.
(41) Lin, H.-P.; Liu, S.-B.; Mou, C.-Y.; Tang, C.-Y. *Chem. Commun.* **1999**, 583.
(42) Tolbert, S. H.; Firouzi, A.; Stucky, G. D.; Chmelka, B. F. *Science* **1997**, *278*, 264.
(43) Göltner, C. G.; Henke, S.; Weissenberger, M. C.; Antonietti, M. *Angew. Chem., Int. Ed.* **1998**, *37*, 613.
(44) (a) Melosh, N. A.; Lipic, P.; Bates, F. S.; Wudl, F.; Stucky, G. D.; Fredrickson, G. H.; Chmelka, B. F. *Macromolecules* **1999**, *32*, 4332. (b) Melosh, N. A.; Davidson, P.; Chmelka, B. F. *J. Am. Chem. Soc.* **2000**, *122*, 823.
(45) Feng, P.; Bu, X.; Stucky, G. D.; Pine, D. *J. Am. Chem. Soc.* **2000**, *122*, 994.
(46) Pevzner, S.; Regev, O.; Yerushalmi-Rozen, R. *Curr. Opin. Colloid Interface Sci.* **2000**, *4*, 420.
(47) (a) Ogawa, M. *J. Am. Chem. Soc.* **1994**, *116*, 7941. (b) Ogawa, M. *Langmuir* **1997**, *13*, 1853. (c) Ogawa, M. *Chem. Commun.* **1996**, 1149.
(48) (a) Ogawa, M.; Ishikawa, H.; Kikuchi, T. *J. Mater. Chem.* **1998**, *8*, 1783. (b) Ogawa, M.; Kikuchi, T. *Adv. Mater.* **1998**, *10*, 1077.
(49) Yang, H.; Kuperman, A.; Coombs, N.; Mamiche-Afara, S.; Ozin, G. A. *Nature* **1996**, *379*, 703.
(50) Aksay, I. A.; Trau, M.; Manne, S.; Honma, I.; Yao, N.; Zhou, L.; Fenter, P.; Eisenberger, P. M.; Gruner, S. M. *Science* **1996**, *273*, 892.
(51) Yang, H.; Coombs, N.; Sokolov, I.; Ozin, G. A. *J. Mater. Chem.* **1997**, *7*, 1285.
(52) Tolbert, S. H.; Schäffer, T. E.; Feng, J.; Hansma, P. K.; Stucky, G. D. *Chem. Mater.* **1997**, *9*, 1962.
(53) Lu, Y.; Ganguli, R.; Drewien, C. A.; Anderson, M. T.; Brinker, C. J.; Gong, W.; Guo, Y.; Soyez, H.; Dunn, B.; Huang, M. H.; Zink, J. I. *Nature* **1997**, *389*, 364.
(54) (a) Zhao, D.; Yang, P.; Margolese, D. I.; Chmelka, B. F.; Stucky, G. D. *Chem. Commun.* **1998**, 2499. (b) Zhao, D.; Yang, P.; Melosh, N.; Feng, J.; Chmelka, B. F.; Stucky, G. D. *Adv. Mater.* **1998**, *10*, 1380.
(55) (a) Yang, H.; Coombs, N.; Sokolov, I.; Ozin, G. A. *Nature* **1996**, *381*, 589. (b) Yang, H.; Coombs, N.; Dag, Ö.; Sokolov, I.; Ozin, G. A. *J. Mater. Chem.* **1997**, *7*, 1755. (c) Yang, H.; Ozin, G. A.; Kresge, C. T. *Adv. Mater.* **1998**, *10*, 883.
(56) Miyata, H.; Kuroda, K. *J. Am. Chem. Soc.* **1999**, *121*, 7621.
(57) Miyata, H.; Kuroda, K. *Chem. Mater.* **2000**, *12*, 49.
(58) (a) Hillhouse, H. W.; Okubo, T.; van Egmond, J. W.; Tsapatsis, M. *Chem. Mater.* **1997**, *9*, 1505. (b) Hillhouse, H. W.; van Egmond, J. W.; Tsapatsis, M. *Langmuir* **1999**, *15*, 4544.
(59) Trau, M.; Yao, N.; Kim, E.; Xia, Y.; Whitesides, G. M.; Aksay, I. A. *Nature* **1997**, *390*, 674.
(60) Melosh, N. A.; Davidson, P.; Feng, P.; Pine, D. J.; Chmelka, B. F. *J. Am. Chem. Soc.* **2001**, *123*, 1240.
(61) Miyata, H.; Kuroda, K. *Adv. Mater.* **1999**, *11*, 1448.
(62) Miyata, H.; Kuroda, K. *Chem. Mater.* **1999**, *11*, 1609.

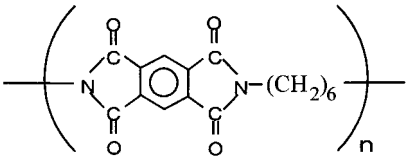

Figure 1. Ideal structure of the polyimide.

by spin coating, and baked at 200 °C for 1 h in an air atmosphere to convert the polyamic acid into a polyimide film.[63] The same polyimide used previously for the preparation of the highly aligned mesoporous silica film[57] was used in this study. The ideal structure of the polyimide is shown in Figure 1. The thickness of the polyimide film was about 100 Å as determined by ellipsometry. The polyimide film on the substrate underwent rubbing treatment using a nylon-covered cylindrical roller (buffing wheel). The details of the rubbing treatment are described in the previous report.[57]

Preparation of the Mesoporous Silica Films. The mesostructured silica film formation was performed through the hydrolysis of silicon alkoxide in the presence of surfactants under acidic conditions.[49,57] Two polyoxyethylene ether nonionic surfactants, $C_{12}EO_{10}$ and $C_{16}EO_{10}$, and a cationic surfactant, C_{16}TAC, were used as templating reagents. Tetraethoxysilane ($(C_2H_5O)_4Si$, abbreviated as TEOS) was mixed with an acidic solution of one of the above surfactants, and the mixture was stirred for 2.5 min at room temperature and transferred into a Teflon vessel. The molar ratio of the reactant solutions was 0.10:0.11:100:8.0: TEOS:surfactant:H_2O:HCl for C_{16}TAC and 0.10:0.11:100:3.0 TEOS:surfactant:H_2O:HCl for the nonionic surfactants, respectively. The rubbing-treated substrate described above was held horizontally in the mixture using a substrate holder with the rubbed polyimide surface downward. The surface of the substrate was covered with another silica glass plate with a 0.2−0.3-mm spacing to obtain a uniform film. The vessel was sealed at 80 °C for 5 days for the formation of the mesostructured silica films. After the reaction, the as-synthesized films were washed with distilled water and dried in air. The calcination of the samples was conducted under an air atmosphere in a muffle furnace at 540 °C for 10 h at a rate of 2 °C min^{-1}.

Characterization. The mesostructured silica films were observed with an optical microscope (Olympus BH2). The porous structure of the films was elucidated by X-ray diffraction (XRD) (Rigaku RAD-2R) using Cu Kα radiation with a graphite monochromator. A grazing angle (the incident angle of X-rays was 0.2°) in-plane XRD study[64] was performed to analyze the mesochannel orientation using an X-ray diffractometer equipped with a 4-axes goniometer (Rigaku ATX-G) with a parabolic multilayer mirror as a primary beam condenser. Cu Kα radiation from a copper rotating anode was used for the experiment, and a soller slit with vertical divergence of 0.48° was used to obtain a parallel beam. Two soller slits with vertical and horizontal divergence of 0.48° were set before the detector to record the $\phi-2\theta\chi$ scanning profiles, whereas only one soller slit with vertical divergence of 0.41° was used to record the ϕ scanning profiles. The two-dimensional XRD patterns were recorded under a reflection geometry using synchrotron radiation at the Photon Factory on beamline 4A. The images of transmission electron microscopy (TEM) were recorded on a Philips Tecnai F30 microscope at an accelerating voltage of 300 kV. The details of the preparation of the specimen for the cross-sectional TEM are described in a previous paper.[57] Nitrogen adsorption isotherms were measured using concomitant powder samples at 77 K on a Quantachrome AUTOSORB-1 gas sorption system. The samples were heated at 150 °C for 4 h in a vacuum prior to the measurements. Pore size distributions were calculated by the BJH method from the adsorption branches of the isotherms.[65]

Results and Discussion

Transparent continuous films were grown on the substrates from each reactant solution described in the Experimental Section. The optimum HCl concentration in the reactant solution for obtaining a transparent film differed with the hydrophilic headgroups of the surfactants. For the cationic surfactant, C_{16}TAC, the optimum concentration was $HCl/H_2O = 7-8/100$, and the concentrations lower than $HCl/H_2O = 7/100$ led to the formation of discrete films as reported previously.[39] However, the HCl concentration optimized for the cationic surfactants, $HCl/H_2O = 7-8/100$, is too high for the nonionic surfactants to provide transparent hexagonal mesostructured silica films. The optimum HCl concentration was $HCl/H_2O = 3/100$ for the nonionic surfactants, though the condition provides mesostructured silica with fiberlike morphology when the cationic C_{16}TAC was employed.[39]

The optical micrographs of the as-grown films are shown in Figure 2. The characteristic texture observed for the mesostructured silica films prepared using C_{16}TAC and $C_{16}EO_{10}$ indicates the preferred alignment of mesochannels perpendicular to the rubbing direction[57] (Figure 2A,C). However, such texture was not observed in the film prepared using $C_{12}EO_{10}$ (Figure 2B). Although no definite texture was observed, partially aligned domains at the discrete part in the film (edge of the film) indicate the structural anisotropy (not shown in Figure 2B) of the film. The mesostructured silica films were not peeled from the substrate by the calcination process for the surfactant removal, even though the underlying polyimide film was lost. No cracks were generated through the calcination process and transparent films were obtained. The adhesive stability of the films onto the silica glass substrate was improved presumably by the formation of Si−O−Si bonds between the film and the substrate through the condensation of mutual silanol groups.

The structure of the films before and after the surfactant removal by calcination was confirmed by XRD. The $\theta-2\theta$ scanning XRD patterns of the films prepared using $C_{12}EO_{10}$ and $C_{16}EO_{10}$ are shown in Figure 3. The patterns of the film prepared using C_{16}TAC are shown in a previous paper[57](see Supporting Information). For each film, the XRD patterns were recorded with two sample geometries; the rubbing direction of the samples was parallel and perpendicular to the incident X-rays. In Figure 3, the diffraction intensity is shown in log scales. In each sample, the diffraction peaks assigned to (100) and (200) of the corresponding two-dimensional hexagonal structure were observed.

The profiles of the films after the calcination process show that the hexagonal channel structure in the films is completely retained after the surfactant removal. The calcination-induced peak shift to higher 2θ positions was observed for all the samples, showing the vertical shrinkage of the structure. The shrinkage should be caused by the condensation of silanol groups in the silica wall. The retention of the hexagonal structure after the removal of the surfactant is in contrast with the

(63) Mittal, K. L. *Polyimides*; Plenum Press: New York, 1984.
(64) Marra, W. C.; Eisenberger, P.; Cho, A. Y. *J. Appl. Phys.* **1979**, *50*, 6927.
(65) Barret, E. P.; Joyner, L. G.; Halenda, P. H. *J. Am. Chem. Soc.* **1951**, *73*, 373.

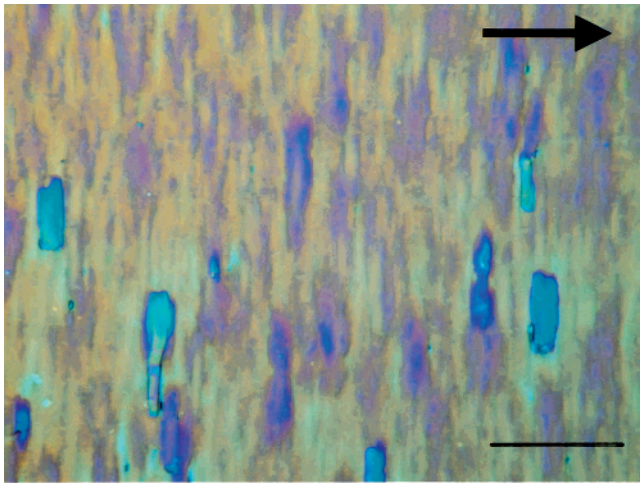

(A)

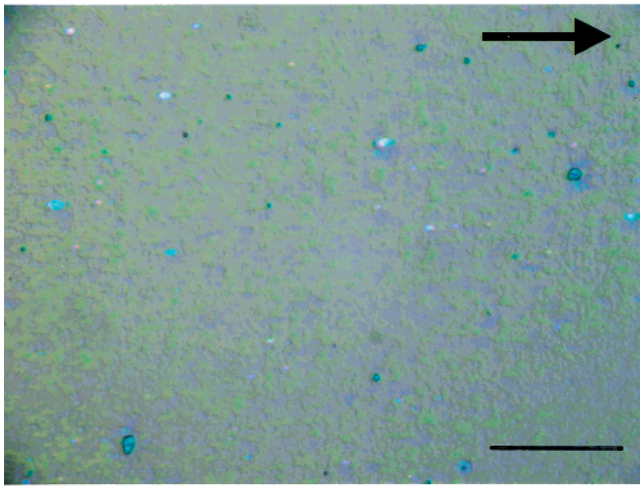

(B)

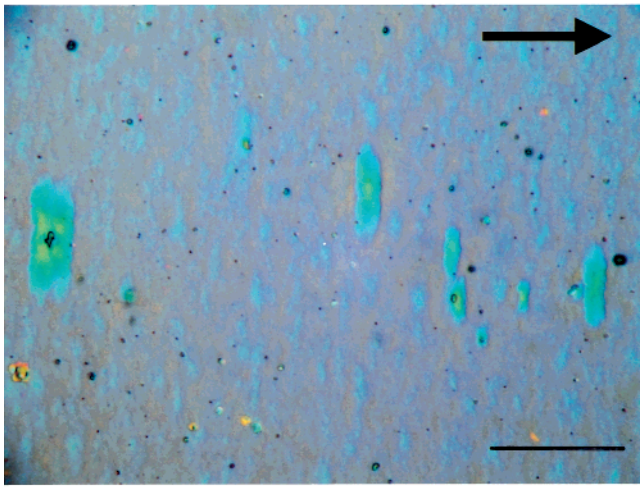

(C)

Figure 2. Optical microscopic images of the as-grown mesostructured silica films prepared using (A) $C_{16}TAC$, (B) $C_{12}EO_{10}$, and (C) $C_{16}EO_{10}$. Arrows show the rubbing directions. Scale bar: 20 μm.

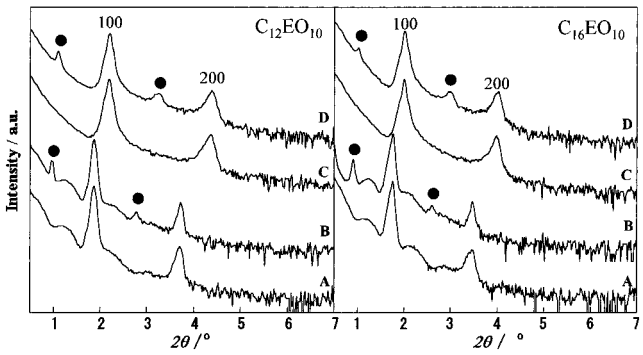

Figure 3. XRD patterns of the mesostructured silica films prepared using $C_{12}EO_{10}$ (left) and $C_{16}EO_{10}$ (right). Profiles A: as-grown films, rubbing direction // X-rays. Profiles B: as-grown films, rubbing direction ⊥ X-rays. Profiles C: calcined films, rubbing direction // X-rays. Profiles D: calcined films, rubbing direction ⊥ X-rays.

previous results on the mesostructured silica film prepared by dip coating using $C_{16}EO_{10}$[66] in which a remarkable structural change was observed through the surfactant removal by a UV−ozone treatment. This inconsistency should be caused by the difference in the degree of polymerization of silica in the wall of the uncalcined films.

In addition to these two peaks, (100) and (200), two extra peaks were observed in each diffraction pattern obtained with the geometry where the rubbing direction was set perpendicularly to the incident X-rays. These extra peaks are marked (●) in the figure. The positions of these extra peaks correspond to the lattice spacings of 2 and 2/3 times of each d_{100} value, which are forbidden for a hexagonal structure. These extra peaks are ascribed to the reciprocal lattice points that do not contribute to the $\theta-2\theta$ scanning XRD under an ideal measurement condition, and it has been shown that the vertical divergence of the incident beam and the small diffraction angle made them detectable.[67] This anisotropy of the XRD patterns is easily understood using two-dimensional XRD patterns. The two-dimensional XRD patterns measured for the calcined mesoporous silica film prepared using $C_{16}EO_{10}$ are shown in Figure 4. The patterns (A) and (B) were recorded with the geometry where the incident X-rays were parallel and perpendicular to the rubbing direction, respectively. The diffraction spots in Figure 4B clearly show that the mesostructured silica film has a single-crystal-like channel structure and that the channels are aligned perpendicularly to the rubbing direction. Although the reciprocal lattice points assigned to (010) and (110) do not contribute to the $\theta-2\theta$ scanning profile under an ideal measurement condition, the diffraction peaks corresponding to these reciprocal lattice points can be observed under the present conditions with a vertical X-ray divergence angle of 5° because the diffraction angle is considerably small compared to the divergence angle. The detailed results on the two-dimensional XRD will be shortly published elsewhere.[67] The fact that these extra peaks are observable only in a peculiar sample direction shows the strong anisotropy of the

(66) Clark, T., Jr.; Ruiz, J. D.; Fan, H.; Brinker, C. J.; Swanson, B. I.; Parikh, A. N. *Chem. Mater.* **2000**, *12*, 3879.
(67) Noma, T.; Miyata, H.; Takada, K.; Iida, A. *Adv. X-ray Anal.* **2001**, *45*, in press.

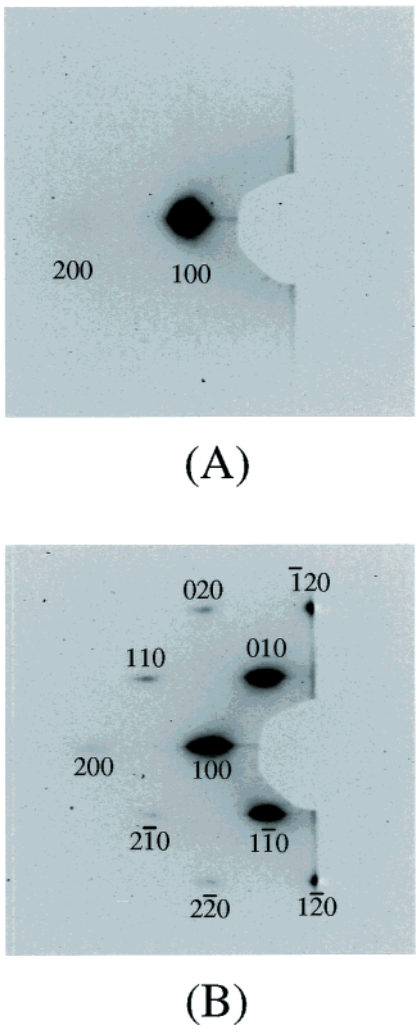

Figure 4. Two-dimensional XRD patterns of calcined mesoporous silica film prepared using $C_{16}EO_{10}$. The rubbing direction was (A) parallel and (B) perpendicular to the incident X-rays.

Table 1. Structure Parameters of the Mesostructured Silica Film with Uniaxially Aligned Mesochannels

sample		d_{100} (Å)	$d_{1\bar{2}0}$ (Å)	$d_{100}/d_{1\bar{2}0}$	fwhm of the ϕ scanning peak (deg)
$C_{12}EO_{10}$	as-grown	47.2	33.3	1.42	15.0
	calcined	40.2	33.5	1.20	12.6
$C_{16}EO_{10}$	as-grown	50.2	37.6	1.34	12.4
	calcined	43.7	37.4	1.17	10.8
$C_{16}TAC$	as-grown	35.6	25.0	1.42	11.5
	calcined	29.2	24.9	1.17	11.1

arrangement of the reciprocal lattice points and is evidence of the highly aligned channel structure. The anisotropy of the XRD patterns is retained after the surfactant removal, indicating the retention of the alignment of the mesochannels.

The lattice spacings of (100) estimated from these XRD patterns are listed in Table 1. Because the solubilities of alkyltrimethylammonium surfactants in an aqueous medium are too low when the number of the alkyl chain exceeds 18, $C_{18}TAC$ will provide the largest mesostructure as long as the conventional cationic surfactants are used. However, the increment of the lattice spacing was small when $C_{18}TAC$ was used in place of $C_{16}TAC$ (see Supporting Information). As

Table 2. Pore Structure Parameters of the Concomitant Mesostructured Silica Powders

sample		d_{100} (Å)	pore size (Å)
$C_{12}EO_{10}$	as-grown	50.8	
	calcined	45.8	35
$C_{16}EO_{10}$	as-grown	56.6	
	calcined	51.1	42
$C_{16}TAC$	as-grown	38.3	
	calcined	35.4	29

shown in Table 1, the use of the nonionic surfactants enables effective enlargement of the periodic structure. The d_{100} value of the as-grown mesostructured silica film prepared using $C_{16}EO_{10}$ is 14.6 Å larger than that of the film prepared using $C_{16}TAC$, though the hydrophobic parts of both surfactants are common. Even the nonionic surfactant with a shorter alkyl chain, $C_{12}EO_{10}$, gave a larger periodic structure than $C_{16}TAC$. These results show that the use of the surfactants with a large hydrophilic part effectively enlarges the periodic structure in the film. However, the use of a nonionic surfactant with a further larger hydrophilic part, $C_{16}EO_{20}$, led to unsuccessful results under similar preparation conditions. This indicates that the size of the hydrophilic part has to be optimized in this strategy for the preparation of mesostructured silica film with aligned mesochannels.

Since the structural period determined by XRD contains the information on the silica wall thickness, experiments of gas adsorption are needed for the estimation of the pore sizes. Nitrogen adsorption experiments were performed using the powder samples that are concomitantly obtained with the mesostructured silica films because the direct estimation of the pore sizes using the thin film samples is too difficult. The average pore sizes estimated by the BJH method along with the d_{100} values of the powder samples are also listed in Table 2. It was clearly shown that the use of the nonionic surfactants led to considerable enlargement of the pore size. However, it must be noted that the channel structure in the films is not identical to that in the powder samples, for example, the d_{100} spacings of the films do not coincide with those of the corresponding powder samples, even though the same surfactants are used. The hexagonal porous structure in the films is distorted, especially in the calcined films, and the horizontal period is particularly longer, as will be discussed later.

The alignment of the mesochannels was quantitatively estimated using grazing incident in-plane X-ray diffraction. The details of in-plane diffraction are described in our previous papers.[56,57,62] The scanning axes of the diffractometer used for in-plane diffraction are schematically drawn in the inset of Figure 5.

The $\phi-2\theta\chi$ scanning profiles of the as-grown mesostructured silica film prepared using $C_{16}EO_{10}$ are shown in Figure 5. The rubbing direction of the sample was parallel (profile A) and perpendicular (profile B) to the incident X-rays at $\phi = 0°$. The in-plane diffraction peak assigned to be $(1\bar{2}0)$ was observed only in the profile B at a position of $2\theta\chi = 2.34°$, showing that the mesochannels are aligned perpendicularly to the rubbing direction. This is substantially identical to the previous result using $C_{16}TAC$.[57] To estimate the distribution of the alignment direction of the mesochannels, the ϕ scanning profile of the $(1\bar{2}0)$ peak intensity was mea-

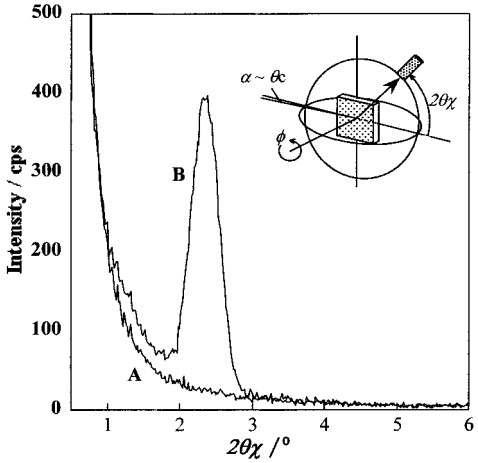

Figure 5. $\phi-2\theta\chi$ scanning profile of the as-grown mesostructured silica film prepared using $C_{16}EO_{10}$. The rubbing direction was (A) parallel and (B) perpendicular to the incident X-rays at $\phi = 0°$. Inset: the scanning axes of the diffractometer for in-plane diffraction measurement.

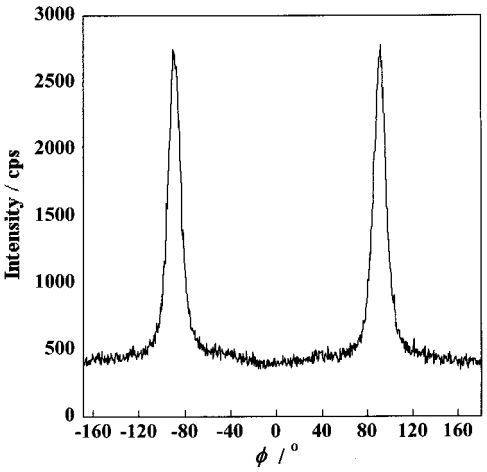

Figure 6. ϕ scanning profile of the as-grown mesostructured silica film prepared using $C_{16}EO_{10}$. The rubbing direction was parallel to the incident X-rays at $\phi = 0°$.

sured. The ϕ scanning profile of the film prepared using $C_{16}EO_{10}$ is shown in Figure 6. The rubbing direction is parallel to the incident X-rays at $\phi = 0°$. The observed profile clearly shows that the mesochannels in the film are aligned perpendicularly to the rubbing direction with very narrow directional distribution. The distribution of the mesochannel alignment was estimated to be 12.4° from the values of the full-width at half-maximum (fwhm) of the diffraction peaks in the ϕ scanning profile.

To confirm the reservation of the mesostructure through surfactant removal, above in-plane XRD measurements were performed for the same film sample after calcination. The $\phi-2\theta\chi$ and ϕ scanning profiles of the calcined mesoporous silica film prepared using $C_{16}EO_{10}$ are shown in Figures 7 and 8, respectively. Although a considerable diffraction peak shift toward higher 2θ positions was observed in the corresponding $\theta-2\theta$ scanning profile through calcination (Figure 3), the peak position in the $\phi-2\theta\chi$ scanning profile was unchanged by calcination (Figures 5 and 7). This means that the shrinkage of the structure is caused only in the vertical direction and the strong adhesion onto the substrate prevents the horizontal structural shrinkage. The comparison of the two ϕ scanning profiles (Figures

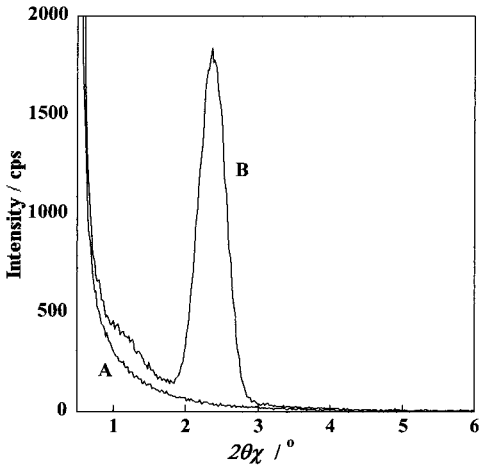

Figure 7. $\phi-2\theta\chi$ scanning profile of the calcined mesoporous silica film prepared using $C_{16}EO_{10}$. The rubbing direction was (A) parallel and (B) perpendicular to the incident X-rays at $\phi = 0°$.

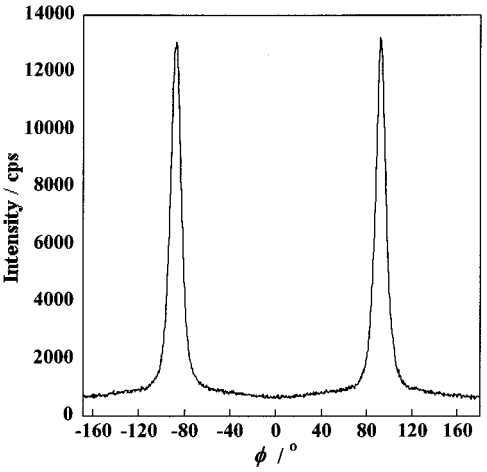

Figure 8. ϕ scanning profile of the calcined mesoporous silica film prepared using $C_{16}EO_{10}$. The rubbing direction was parallel to the incident X-rays at $\phi = 0°$.

6 and 8) recorded before and after calcination shows that the alignment of the mesochannels is completely preserved through calcination. The fwhm of the diffraction peak in Figure 8 is slightly narrower than that observed for the as-grown film (see Table 1). The reason for the observed narrowing in the directional distribution of the mesochannels by calcination is not clear but it would be related to the change in the density distribution.

A series of above in-plane XRD measurements were also performed for the other two films prepared using $C_{12}EO_{10}$ and $C_{16}TAC$.[57] Both of the films provided substantially the same profiles as those observed for the film prepared using $C_{16}EO_{10}$ apart from the peak positions in the $\phi-2\theta\chi$ scanning profiles. From these results, it was confirmed that the highly aligned channel structure is achieved in all the films.

The lattice spacings of $(1\bar{2}0)$ estimated from each $\phi-2\theta\chi$ scanning profile, which correspond to half the horizontal distance between the neighboring pores, are listed in Table 1. The observed spacings of $(1\bar{2}0)$ are considerably larger than the values calculated from the corresponding (100) spacings on the assumption of an ideal hexagonal structure, showing the hexagonal structure in the films is distorted. The pore distance along

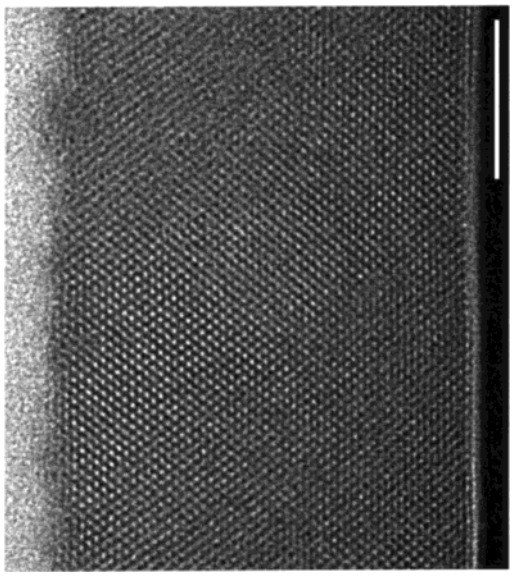

Figure 9. Cross-sectional TEM image of the as-grown mesostructured silica film prepared using $C_{16}EO_{10}$. The film was sliced parallel to the rubbing direction. Scale bar: 100 nm.

the horizontal axis is peculiarly longer than those along the other two directions. Crystallographically, this phase is not hexagonal but orthorhombic. Because the shrinkage of the structure by calcination is caused only in the vertical direction, the distortion of the hexagonal structure is amplified by calcination. To quantitatively estimate the distortion of the hexagonal structure, the d_{100}/d_{120} ratio, which is equal to 1.73 for an ideal hexagonal structure, was calculated for the each sample and listed in Table 1. Interestingly, it was found that the ratios are almost independent of the surfactants used both for the as-grown and calcined films. This would be explained by interfacial interactions between the polymer chains of the rubbed polyimide and the surfactants. At the interface, the adsorbed surfactant molecules would be elongated by a certain degree, comparing with the length of the corresponding "free" surfactant molecules through the interactions. The lattice spacings of $(1\bar{2}0)$ in the films are larger than those in the corresponding powder samples, and on the other hand, the spacings of (100) in the films are smaller than those in the powder samples. The smaller vertical distances in the films would be the consequence of the compensation of the horizontal elongation to keep the micelle volumes constant.

The fwhm values of the peaks in the ϕ scanning profiles are also listed in Table 1. It was found that the distribution of the alignment direction is nearly independent of the surfactants used. This means that the alignment distribution of the mesochannels is determined mainly by the degree of the rubbing-induced structural anisotropy of the underlying polymer. Particularly, the distributions of the alignment direction estimated for the two films prepared using $C_{16}TAC$ and $C_{16}EO_{10}$, surfactants with different hydrophilic groups and the same hydrophobic alkyl chains, are very close to each other. This shows that the hydrophobic tail groups of the surfactants mainly contribute to the surface micelle alignment through the hydrophobic interactions with the anisotropic polymer chains. The alignment distribution in the film prepared using $C_{12}EO_{10}$ is slightly wider than that in the corresponding film prepared using $C_{16}EO_{10}$. This is consistent with the above assumption that the hydrophobic interactions at the interface determine the mesochannel alignment because the hydrophobic interactions should be stronger for the surfactants with longer alkyl chains.

Figure 9 is a cross-sectional TEM image of the as-grown mesostructured silica film prepared using $C_{16}EO_{10}$. The sample was sliced parallel to the rubbing direction. The honeycomb structure of the mesochannels is observed over all thicknesses of the film, demonstrating perfectly aligned mesostructure. In this image, the distortion of the hexagonal structure is obvious. The lattice distance along the horizontal axis is peculiarly longer than those along the other two directions, which is consistent with the results of the XRD discussed above.

In the present study, it was found that the distribution of the alignment direction of the mesochannels in the mesostructured silica films was independent of the hydrophilic part of the surfactants and that the surfactant with a shorter alkyl chain provides wider distribution. Again, the degree of the distortion of the hexagonal porous structure in the films was found to be independent of the surfactants. These results strongly support the previously reported alignment mechanism[57,61] in which the hydrophobic interactions between the polymer chains of the rubbed polyimide and the surfactant tail groups lead to the formation of aligned hemicylindrical micelles at the polymer surface.

Conclusion

The combination of the rubbing-treated polyimide coating with optimum chemical structure and the optimum nonionic surfactants led to a successful formation of mesoporous silica films with highly aligned large mesochannels. The hexagonal channel structures in the films are distorted by means of the interfacial interactions, and the degree of the distortion was independent of the surfactants used. The distribution of the channel direction in the film is independent of the hydrophilic part in the surfactants but is slightly affected by the length of the hydrophobic alkyl chains. These results support the alignment mechanism that the hydrophobic interactions between the polymer chains of the rubbed polyimide and the surfactant tail groups lead to the formation of the aligned hemicylindrical micelles at the interfaces.

Acknowledgment. The authors acknowledge Mr. S. Fujita and Ms. M. Asaki (Yuasa Ionics Co.) for the nitrogen adsorption measurements. The authors also acknowledge Prof. A. Iida (Photon Factory) for useful discussion on the two-dimensional XRD results. This work was partially supported by a Grant-in-Aid for COE Research, MEXT, Japan.

Supporting Information Available: Figure of XRD patterns of the mesostructured silica films prepared using $C_{16}TAC$ and $C_{18}TAC$ and table of d_{100} values estimated from the XRD patterns (PDF). This material is available free of charge via the Internet at http://pubs.acs.org.

CM010412M